Article

Thalamus drives vocal onsets in the zebra finch courtship song

Felix W. Moll[1,2,3], Devorah Kranz[1,2], Ariadna Corredera Asensio[1,2], Margot Elmaleh[1,2], Lyn A. Ackert-Smith[1,2] & Michael A. Long[1,2 ✉]

While motor cortical circuits contain information related to specific movement parameters[1], long-range inputs also have a critical role in action execution[2,3]. Thalamic projections can shape premotor activity[2–6] and have been suggested[7] to mediate the selection of short, stereotyped actions comprising more complex behaviours[8]. However, the mechanisms by which thalamus interacts with motor cortical circuits to execute such movement sequences remain unknown. Here we find that thalamic drive engages a specific subpopulation of premotor neurons within the zebra finch song nucleus HVC (proper name) and that these inputs are critical for the progression between vocal motor elements (that is, 'syllables'). In vivo two-photon imaging of thalamic axons in HVC showed robust song-related activity, and online perturbations of thalamic function caused song to be truncated at syllable boundaries. We used thalamic stimulation to identify a sparse set of thalamically driven neurons within HVC, representing ~15% of the premotor neurons within that network. Unexpectedly, this population of putative thalamorecipient neurons is robustly active immediately preceding syllable onset, leading to the possibility that thalamic input can initiate individual song components through selectively targeting these 'starter cells'. Our findings highlight the motor thalamus as a director of cortical dynamics in the context of an ethologically relevant behavioural sequence.

The songbird is an advantageous model system for understanding the neural mechanisms underlying a learned complex behaviour. During singing, adult male zebra finches produce a fixed sequence of typically 2–7 'syllables', which represent functionally[9,10] and developmentally[11] distinct motor elements. The motor thalamic nucleus Uvaeformis (Uva) has been shown to be a critical node in the vocal production pathway necessary for singing[12–17]. In line with these results, we found that vocalizations following Uva lesions (n = 6 birds)—but not sham lesions (n = 2 birds)—became diffuse and no longer categorically distinct (that is, the syllable structure was lost) (Fig. 1b,c and Extended Data Fig. 1). Uva provides input to the cortical nucleus HVC through direct projections as well as indirectly through the nucleus interfacialis of the nidopallium (NIf)[17] and Avalanche (Av)[18] (Fig. 1a). During singing, intrinsic circuitry within HVC[16,19–22] generates a sparse sequence of activity tiling the entirety of song[23], with each premotor neuron contributing a burst at a single invariant time point relative to the song[24,25]. By using this sparse HVC code as a temporal readout, we examine the functional connections from Uva to HVC to assess the impact of motor-related thalamic circuitry in the context of an ethologically relevant complex behaviour.

Perturbation of thalamus during singing

Although the principal necessity for Uva activity had long been established[12–17], the dynamic role of this activity in vocal production remains an important point of disagreement. Uva has been proposed to be part of a fast feedback loop during singing (that is, the 'fast feedback model') whose persistent activity is required to propagate moment-to-moment sequence generation in HVC[26]. In the alternative 'initiation model', Uva activity may provide a 'go cue' for song-related HVC sequences[27,28], which can then propagate without the need for additional thalamic drive[16]. These models make distinct predictions concerning the impact of an 'online' perturbation during singing: the fast feedback model predicts that Uva perturbations will lead to an indiscriminate song truncation at all time points, whereas the initiation model predicts that the impact of Uva perturbations will be restricted to specific moments within the song (that is, syllable boundaries).

To test these hypotheses, we manipulated ongoing network activity using electrical microstimulation (five pulses at 500 Hz; current range, 20–120 µA) administered bilaterally during singing. When applied to HVC, this manipulation profoundly suppressed local activity for ~200 ms (n = 64 neurons from two birds), probably through the activation of local inhibitory interneurons (Extended Data Fig. 2), in line with previous observations in other circuits[29,30], including thalamus[30]. In singing birds, bilateral stimulation of Uva (Fig. 1d and Extended Data Fig. 3a–d) led to truncations at the end of syllables (Fig. 1e and Extended Data Fig. 3e–h) (n = 4 birds; modal latencies of 47, 49, 60 and 71 ms). Additionally, song was interrupted at discrete transition points near the centre of long-duration, complex syllables (Extended Data Fig. 3e–h), in line with previous observations that such

[1]NYU Neuroscience Institute and Department of Otolaryngology, New York University Langone Medical Center, New York, NY, USA. [2]Center for Neural Science, New York University, New York, NY, USA. [3]Animal Physiology, Institute of Neurobiology, University of Tübingen, Tübingen, Germany. ✉e-mail: mlong@med.nyu.edu
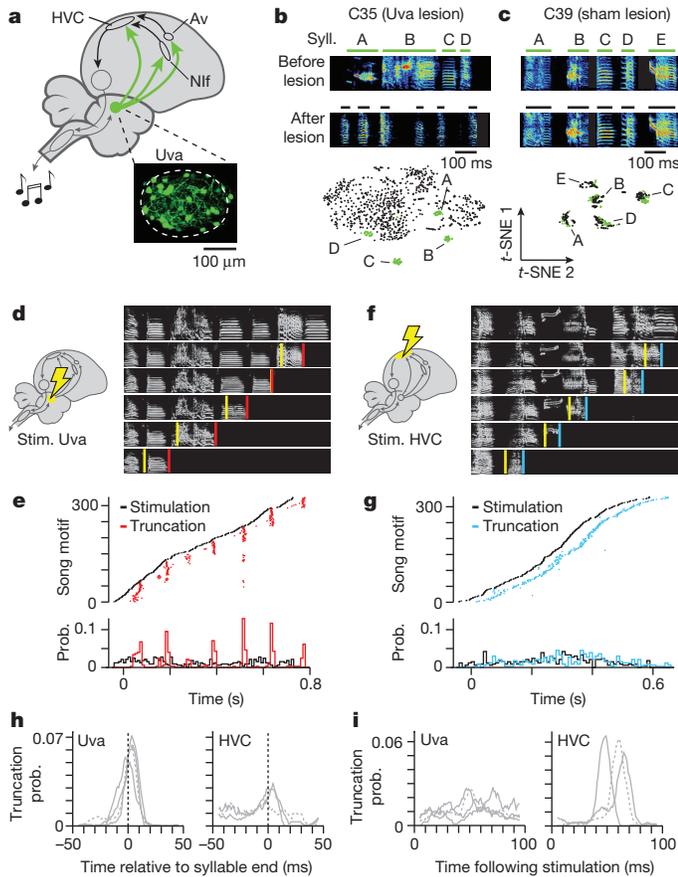
Fig. 1 | Uva perturbations impact normal syllabic song structure.
a, Schematic of the zebra finch song control pathway (sagittal view), including HVC, Uva, NIf and Av. The inset shows a histological slice through Uva with GFP-labelled HVC-projecting neurons ($n = 3$ birds). **b,c**, Example sonograms from two individual zebra finches before (top) and after (bottom) a unilateral Uva lesion (**b**) or a similarly sized lesion located outside of Uva (**c**). Vocalizations produced by each bird are represented by single points in a *t*-distributed stochastic neighbour embedding (*t*-SNE) plot at the bottom (green, before lesion; black, after lesion). Syll., syllable. **d**, Example songs truncated by bilateral Uva stimulation (stim.). Yellow lines, stimulation times; red lines, song truncation times. Reference song at top. **e**, Uva stimulation and song truncation times (black and red ticks, respectively; $n = 325$ trials) for all stimulated trials resulting in a truncation aligned to the sonogram in **d**. Bottom, the probability (prob.) of stimulation and song truncation (black and red lines, respectively). **f**, Example songs truncated by bilateral HVC stimulation. **g**, HVC stimulation and song truncation times (black and blue ticks, respectively; $n = 331$ trials) aligned to the sonogram in **f**. **h,i**, Probability of song truncation related to closest syllable offset (**h**) or stimulation time (**i**) following Uva ($n = 4$ birds, left) or HVC ($n = 3$ birds, right) stimulation. Each line represents data from a single bird; dashed lines refer to birds shown in **e** and **g**, respectively.

syllables are often composed of smaller (~100–150 ms) functional elements[10,22]. Similar effects were observed when we stimulated Uva unilaterally in two birds (Extended Data Fig. 3l,m). Conversely, an equivalent, bilateral perturbation administered to HVC (reanalysed data from ref. [31]) truncated singing throughout the entirety of the song (Fig. 1f,g and Extended Data Fig. 3i–k) with a modal latency of ~60 ms (range, 49–65 ms; $n = 3$ birds), in agreement with previous results[32,33]. Uva and HVC stimulation-related truncation time distributions were significantly different when aligned to either the end of syllables (Fig. 1h) or the time of the stimulation (Fig. 1i) (Kruskal–Wallis test, $P < 0.0001$ and $P < 0.01$, respectively). The truncation of song at syllable boundaries following Uva perturbation indicates that
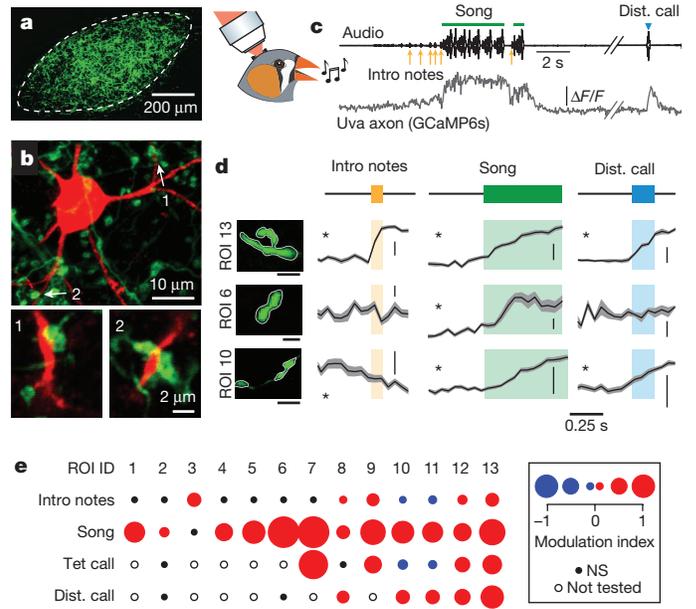

Fig. 2 | Structure and function of thalamic inputs to HVC. a, GFP-labelled Uva axons densely innervate HVC (borders indicated with dashed white line). **b**, Top, GFP-labelled Uva axons located near a single HVC premotor neuron (tdTomato). Bottom, a closer view of putative synaptic connections 1 (*z* stack = 4 μm) and 2 (*z* stack = 2.5 μm) indicated above ($n = 2$ birds). **c**, Single-trial activity of an Uva axon labelled with GCaMP6s. Raw audio trace shown above; axonal fluorescence of ROI 13 shown below ($\Delta F/F$ scale bars, 1). Dist. call, distance call; intro notes, introductory notes. **d**, GCaMP6s activity from three example Uva axons. ROIs indicated by white lines in the micrographs on the left (scale bars: ROI 13, 5 μm; ROI 6, 2 μm; ROI 10, 10 μm). Average and s.e.m. fluorescence traces aligned to vocal onsets ($\Delta F/F$ scale bars: intro notes, 0.1; song, 0.4; distance call, 0.4). Asterisks denote significant responses. **e**, The modulation index indicates response strength for all imaged axons ($n = 2$ birds; blue, decrease; red, increase; black, not significant (NS)).

thalamic activity is critical for starting the following syllable but not for completing the ongoing syllable, in line with the initiation model introduced above.

HVC receives song-related thalamic input

After demonstrating a role for Uva in the initiation of song elements, we next examined the anatomical features of the Uva-to-HVC thalamocortical pathway. We first quantified the number of Uva neurons directly projecting to HVC. Using an intersectional retrograde approach (Methods), we counted 739, 643 and 887 HVC-projecting Uva (Uva$_{HVC}$) neurons in the ipsilateral hemisphere of three zebra finches (Extended Data Fig. 4). We then turned our attention to the impact of these Uva inputs into HVC. Anterograde labelling of Uva neurons with green fluorescent protein (GFP) showed widespread thalamic innervation throughout the extent of HVC (Fig. 2a). Furthermore, at a single-neuron level, large axonal swellings (likely synaptic boutons) from Uva were observed near the soma and dendrites of some premotor HVC neurons (Fig. 2b), suggesting direct synaptic connections to these cells[13].

A simple prediction from our behavioural result is that thalamic inputs to HVC will be modulated during singing. In prior electrophysiological studies of Uva[14,15], no efforts were made to distinguish the contribution of specific projection neuron subtypes (to HVC, to NIf or to Av) from the activity of local circuit interneurons. To test whether HVC-projecting Uva neurons exhibit vocalization-related responses, we expressed the calcium indicator GCaMP6s in Uva and used two-photon imaging to examine the activity of individual thalamic

Article
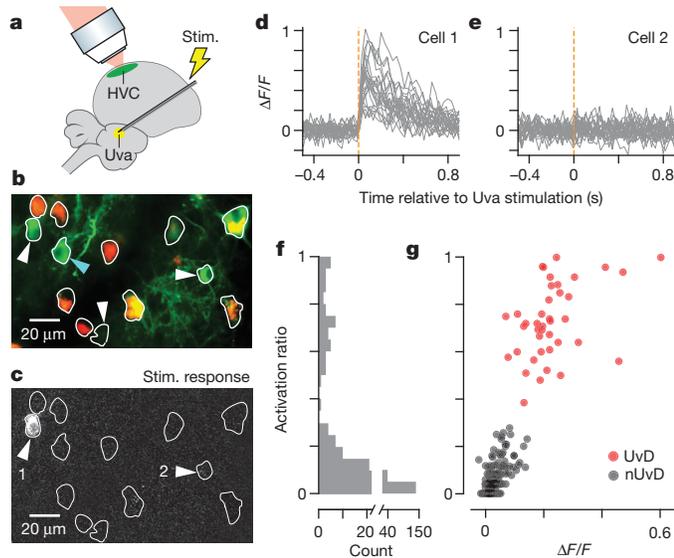
Fig. 3 | Classifying HVC premotor neurons on the basis of thalamic drive.
a, Schematic depicting simultaneous in vivo two-photon imaging in HVC along with electrical microstimulation in Uva. **b**, In vivo two-photon image of an example plane featuring GCaMP6s-labelled somata (white outlines, ROIs; white arrowheads, HVC premotor neurons; blue arrowhead, HVC interneuron; red soma label, basal ganglia-projecting HVC neurons) ($n = 6$ birds). **c**, Average fluorescence changes following 25 Uva stimulation events; only cell 1 shows significant response ($n = 6$ birds). **d,e**, HVC premotor neuron examples from **c** that are driven (**d**) or not driven (**e**) by Uva stimulation. **f,g**, Distribution of activation ratios (**f**) and a scatterplot displaying activation ratios and stimulation-evoked $\Delta F/F$ (**g**) for 251 HVC premotor neurons. Colours indicate functional distinction as UvD or nUvD neurons following a clustering procedure (Methods).

axons in HVC during vocalization (Fig. 2c). Uva inputs recorded from two birds displayed heterogeneous responses across a range of vocal types (Fig. 2d,e), as determined by the 'modulation index', or the proportion of trials in which a significant increase (1) or decrease (−1) in fluorescence was detected (Methods). Specifically, we found that 12 of 13 regions of interest (ROIs) responded significantly during singing, while only 7 changed their activity during introductory notes (5 increasing and 2 decreasing), which typically precede song. Thalamic axons also sometimes increased their activity during calls, vocalizations that are distinct from song (distance call, 5 of 7 ROIs; tet call, 4 of 8 ROIs) (Fig. 2e). In sum, these results indicate that, although thalamic inputs to HVC exhibit some selectivity across the zebra finch vocal repertoire, they appear to be universally activated during song.

Thalamically driven HVC subpopulation

Our next step was to estimate the impact of thalamic activation on downstream HVC circuitry in the context of song by functionally identifying neurons within HVC that were driven by thalamic activity. To accomplish this, we expressed GCaMP6s in HVC neurons and used two-photon imaging to monitor Uva stimulation-evoked responses in HVC ($n = 6$ birds) (Fig. 3a). We imaged different HVC cell types as defined by retrograde tracers and functional criteria (Methods). In addition to HVC premotor neurons, which project to the robust nucleus of the arcopallium (RA), or HVC_{RA} neurons ($n = 251$), we also imaged HVC neurons projecting to the avian basal ganglia called Area X (HVC_X neurons, $n = 667$) (Fig. 3b). The remaining neurons ($n = 351$) had functional profiles inconsistent with these cell classes and may represent either local inhibitory interneurons[25] or members of a considerably smaller population of cells projecting to Av (HVC_{Av} neurons)[34]. In line with previous findings[13], electrical stimulation in Uva resulted

in short-latency, stimulus-locked activation in a subset of HVC neurons (for example, cell 1 in Fig. 3c,d) independently of the state of the bird (that is, awake or ketamine anaesthetized; Methods), while most imaged neurons showed no stimulation-induced fluorescence changes (for example, cell 2 in Fig. 3c,e).

We established a quantitative metric to identify putative thalamorecipient HVC neurons. Specifically, we calculated an 'activation ratio' consisting of the proportion of trials with significant stimulation-induced responses across trials (24.8 ± 7.0 stimulation trials per neuron; Methods). We found a bimodal distribution of activation ratios in our population of HVC_{RA} premotor neurons (Fig. 3f) but not in HVC_X or 'HVC interneurons + HVC_{Av} neurons' (Extended Data Fig. 5a–c). We then used k-means clustering to assign each premotor neuron ($n = 251$ from $n = 6$ birds) to one of two populations: 'Uva-driven' (UvD) cells activated by Uva stimulation (15.9%; median latency = 5.8 ms; Extended Data Fig. 5d) and cells that were 'not Uva driven' (nUvD) (Fig. 3g). Because only a small subset of cells was driven by Uva stimulation, these results indicate that thalamic input primarily targets a specific subgroup of premotor neurons within HVC.

Function of thalamus-driven HVC neurons

Once the premotor neurons had been classified as either UvD or nUvD cells, we revisited these neurons to determine their activity profile in the singing bird (Fig. 4a–c and Supplementary Video 1). The vast majority (99.2%) of song-related HVC neurons classified as premotor (that is, both UvD and nUvD cells) produced a single, extremely reliable phasic increase in fluorescence for each rendition of song, whereas 29.4% of neurons labelled with a retrograde marker from Area X exhibited multiple phasic increases, consistent with previous electrophysiological recordings[24,25]. We used an established Bayesian inference method[23] to pinpoint the burst onset time across multiple song trials (27.6 ± 13.2 trials per neuron) (Fig. 4d). This approach enabled us to estimate the timing of song-related activity for individual premotor neurons with sufficient temporal precision (temporal uncertainty, 2.9 ± 1.4 ms) to characterize the activity profiles of UvD and nUvD neurons in relation to vocal production (Fig. 4e,f).

If the thalamic nucleus Uva has a role in vocal initiation, the activity of UvD neurons should be non-uniformly distributed throughout the song (that is, active before vocal onsets). Our song perturbation results (Fig. 1) and previous work[27] suggest that the brief (~20–50 ms) inspiratory pulses preceding syllable onsets could be relevant landmarks in this regard. Upon initial inspection, we observed that UvD neuron activity appeared clustered around these silent periods preceding syllables or shortly before local amplitude minima of long-duration, complex syllables, while the activity of nUvD neurons did not correspond to these features (Fig. 4g and Extended Data Fig. 6a–f). To quantify this difference, we calculated the median event-triggered song amplitude for both the UvD and nUvD populations (Fig. 4h–k). UvD events were associated with a significant dip in song amplitude from 4 to 19 ms (that is, exceeding the 99% confidence interval of a uniform distribution; Methods) (Fig. 4h,i and Extended Data Fig. 6g). Conversely, the song amplitude did not vary as a function of the timing of nUvD spiking events, as expected for event times that are uniformly distributed across the song (Fig. 4j,k and Extended Data Fig. 6). Furthermore, the event-triggered song amplitude associated with the UvD population (window, 0–25 ms) was significantly lower than that associated with the nUvD population (Wilcoxon two-sided test, $P < 0.05$). Taken together, these results demonstrate that UvD population firing is associated with minima in the song amplitude profile, consistent with moments where syllable initiation is likely to occur.

To directly test the notion that UvD firing events cluster around vocal boundaries, we examined the timing of these neurons with respect to the onsets and offsets of song syllables and other vocal behaviours, specifically introductory notes and calls (Fig. 4l,m and Extended Data
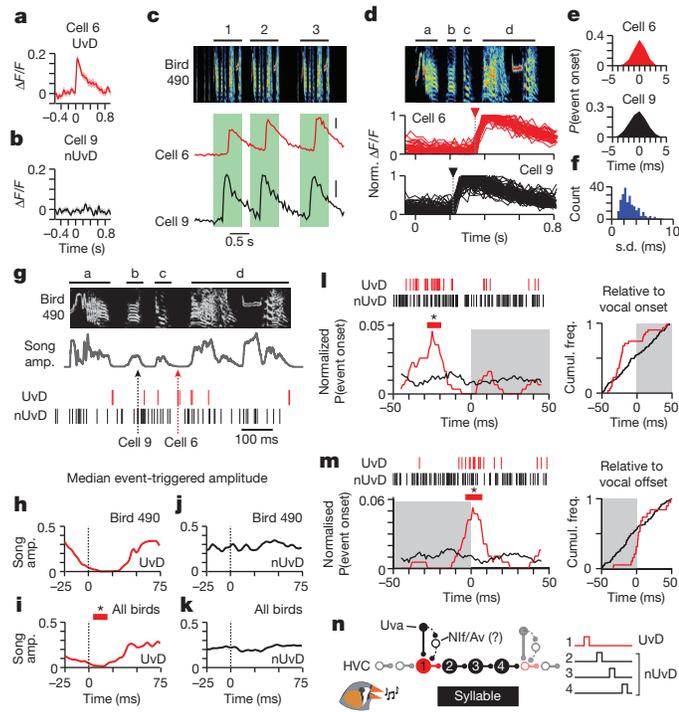
Fig. 4 | Differential roles of UvD and nUvD neurons during song production. **a**,**b**, Average response of two example premotor neurons to Uva stimulation (cell 6, $n = 50$ trials; cell 9, $n = 74$ trials; shading represents s.e.m.). **c**, GCaMP6s responses during singing ($\Delta F/F$; scale bar, 100%) for the two HVC premotor neurons highlighted in **a** and **b**. **d**, Song-related activity of cells 6 ($n = 41$ trials) and 9 ($n = 66$ trials) aligned to song motif. The dashed line indicates the estimated median spiking event onset time. Traces normalized (norm.) by maximum value. **e**, Distribution of spiking event time estimates (Methods) relative to the median estimate for cells 6 and 9. **f**, Distribution of spiking event time uncertainties for all 241 HVC premotor neurons active in the context of vocal production. **g**, Spiking event times for UvD ($n = 11$) and nUvD ($n = 58$) neurons (red and black ticks, respectively) in bird 490 aligned to the sonogram and song amplitude (amp.). Arrows indicate the song-related event times of cells 6 and 9 shown in **d**. **h**–**k**, Median normalized song amplitude envelopes aligned to UvD and nUvD spiking event times for bird 490 (**h**,**j**) and all six birds (**i**,**k**) (UvD, $n = 30$ events; nUvD, $n = 174$ events). The zero point represents the timing of each HVC_{RA} neuron's spiking event. The red bar in **i** indicates the time for which the envelope exceeds the 99% confidence interval (Methods). **l**,**m**, Spiking event times aligned to vocal onsets (**l**) or offsets (**m**) for UvD and nUvD HVC premotor neurons ($n = 6$ birds). Shading indicates presence of vocalization. Horizontal red lines indicate moments in which the population exceeds 99% confidence interval of a uniform distribution. Syllable, introductory note and call-related event times were pooled; see Extended Data Fig. 7a,b for each vocal type analysed separately. Cumul. freq., cumulative frequency. **n**, Uva preferentially engages a subpopulation of HVC 'starter neurons' (in red) directly or through NIf or Av to initiate syllables.

Fig. 7a,b). We therefore use the term 'vocal onsets and offsets' inclusively to refer to all these vocal types. We found that nUvD spiking events were uniformly distributed within our analysis window (±50 ms relative to vocalization) whereas UvD spiking events consistently occurred ~25 ms before vocal onsets (Fig. 4l and Methods), roughly equivalent to the delay inherent between HVC premotor commands and song production[35]. We then aligned responses with respect to vocal offsets and found that the activity of UvD neurons (but not nUvD neurons) was clustered at this boundary as well (Fig. 4m), potentially serving as a stop signal or a go cue for the following syllable or song motif[35]. We observed cases in which UvD neurons were active at the end of the last syllable of song as well as in advance of the first syllable, in line with UvD premotor neuron activity mediating both stop and start signals (Extended Data

Fig. 8). Notably, the state of the bird during our functional classification of thalamorecipient neurons had no bearing on the outcome; we observed significant clustering of song-related spiking activity around vocal boundaries for neurons designated as Uva driven in both awake and ketamine-anaesthetized birds (Extended Data Fig. 7c,d). Additionally, syllable onset activity was observed in HVC_X neurons (Extended Data Fig. 7e), whose role in singing behaviour in the adult bird remains unclear[36]. Taken together, these data indicate that the thalamic nucleus Uva is preferentially capable of activating cortical neurons that represent vocal boundaries and are therefore well positioned to initiate or terminate behaviourally relevant network activity.

Discussion

Our results support a conceptual model in which thalamic inputs from Uva can selectively engage specific elements within a cortical premotor circuit to direct vocal behaviour (Fig. 4n). To accomplish this, Uva could drive HVC neurons directly through the large synaptic inputs that we found to be active during song production (Fig. 2). Uva may also exert its influence through NIf or Av, nuclei that are important for song learning and auditory processing[34,37] but that—unlike Uva[12–16]—appear to have a considerably lesser role in adult courtship song production[38,39]. The temporal clustering of UvD neurons along with the Uva perturbation results is inconsistent with existing models requiring continuous thalamic activation for song production[26]. Instead, we provide a compelling biological example of a recent theoretical proposal[7] in which thalamic inputs can precisely initiate individual elements within the context of a skilled behavioural sequence.

Uva is embedded within a complex song production network. In addition to the multiple postsynaptic targets described above, it also receives input from the dorsomedial nucleus (DM) of the intercollicular complex and nucleus parambigualis (PAm), a respiratory premotor centre in the medulla[33]. Electrical stimulation in Uva may therefore activate these upstream regions antidromically or trigger other descending fibres (for example, from RA) passing nearby, which may complicate the interpretation of our behavioural observations. However, previous work has demonstrated that direct stimulation of either PAm[33] or RA[32,33] results in fixed-latency song interruptions, like those observed following HVC stimulation and categorically different from what we report following Uva stimulation. Additionally, although the song-related activity in DM and PAm has not yet been characterized, signals arising from these upstream nuclei must first pass through Uva to interface with the HVC premotor network, further reinforcing the role of the thalamic nucleus Uva as an important functional bottleneck.

Our findings have demonstrated that thalamocortical inputs can mediate their effect through preferential wiring onto a key premotor population. We have also unveiled new testable hypotheses regarding the nature of this thalamic engagement of cortical circuitry. First, although the timing of Uva and NIf neuron activity[14,15,40] and depolarizing postsynaptic potentials in HVC neurons[26] appears to favour syllable boundaries, activity is consistently found at multiple times throughout the song. How can this broader activity translate into a single, precise spiking event, for instance, at the level of an HVC 'starter neuron' (that is, UvD neurons active at the beginning of a vocalization) (Fig. 4n)? One hypothesis is that multiple co-active thalamic inputs must converge on a single HVC neuron to initiate a downstream response. Alternatively or in addition, gaps in inhibition mediated by local HVC interneurons could provide sparse permissive windows during which thalamic input can effectively drive individual HVC premotor neurons[41,42]. In line with this notion, local minima in interneuron firing rates have been observed to precede syllable onsets in singing birds[25]. Likewise, starter neurons may be more excitable than other cells within the HVC circuit[43], which could facilitate their activation. Finally, HVC_X neurons, which were less robustly driven by Uva stimulation than HVC_{RA} neurons (Extended Data Fig. 5a,b), could have a role in relaying Uva

Article

drive to HVC premotor neurons[19,21]. These factors may further explain the ability of thalamic drive to initiate local HVC dynamics that lead to the formation of individual vocalizations.

In conclusion, our results highlight a mechanism by which motor thalamus can initiate cortical dynamics to generate a complex motor sequence, an arrangement that carries several systems-wide advantages. Uva is well positioned to coordinate bilateral activity at key moments in the song, which can provide an important synchronizing cue given the lack of interhemispheric projections in the cortical song motor pathway[28]. Furthermore, Uva relays dense inputs from the brainstem respiratory centres to HVC[44], and this feedback probably aids in the integration of breathing and vocal production[45]. A similar arrangement has been suggested for the coordination of human speech and respiration[46–48], but direct anatomical pathways supporting this hypothesis have so far not been described. Future work can investigate how sensory inputs—including those contributing to the well-characterized visual responses in Uva—may exploit this wiring to initiate singing behaviour[49]. In addition, the role of Uva in motor initiation is reminiscent of recent rodent studies[2,3], which have demonstrated the necessity of thalamic input to motor cortex for cued movements. Specifically, thalamic input can provide a brief go cue that rapidly reorganizes cortical dynamics from a motor planning to a motor execution phase[2]. Taking this together with our present results, thalamus appears to act as a critical initiator of premotor sequences and their corresponding behaviours across vertebrate taxa.

Online content

Any methods, additional references, Nature Portfolio reporting summaries, source data, extended data, supplementary information, acknowledgements, peer review information; details of author contributions and competing interests; and statements of data and code availability are available at https://doi.org/10.1038/s41586-023-05818-x.

1. Shenoy, K. V., Sahani, M. & Churchland, M. M. Cortical control of arm movements: a dynamical systems perspective. *Annu. Rev. Neurosci.* **36**, 337–359 (2013).
2. Inagaki, H. K. et al. A midbrain–thalamus–cortex circuit reorganizes cortical dynamics to initiate movement. *Cell* **185**, 1065–1081 (2022).
3. Dacre, J. et al. A cerebellar–thalamocortical pathway drives behavioral context-dependent movement initiation. *Neuron* **109**, 2326–2338 (2021).
4. Guo, Z. V. et al. Maintenance of persistent activity in a frontal thalamocortical loop. *Nature* **545**, 181–186 (2017).
5. Gaidica, M., Hurst, A., Cyr, C. & Leventhal, D. K. Distinct populations of motor thalamic neurons encode action initiation, action selection, and movement vigor. *J. Neurosci.* **38**, 6563–6573 (2018).
6. Sauerbrei, B. A. et al. Cortical pattern generation during dexterous movement is input-driven. *Nature* **577**, 386–391 (2020).
7. Logiaco, L., Abbott, L. F. & Escola, S. Thalamic control of cortical dynamics in a model of flexible motor sequencing. *Cell Rep.* **35**, 109090 (2021).
8. Tanji, J. Sequential organization of multiple movements: involvement of cortical motor areas. *Annu. Rev. Neurosci.* **24**, 631–651 (2001).
9. Glaze, C. M. & Troyer, T. W. Temporal structure in zebra finch song: implications for motor coding. *J. Neurosci.* **26**, 991–1005 (2006).
10. Cynx, J. Experimental determination of a unit of song production in the zebra finch (*Taeniopygia guttata*). *J. Comp. Psychol.* **104**, 3–10 (1990).
11. Okubo, T. S., Mackevicius, E. L., Payne, H. L., Lynch, G. F. & Fee, M. S. Growth and splitting of neural sequences in songbird vocal development. *Nature* **528**, 352–357 (2015).
12. Coleman, M. J. & Vu, E. T. Recovery of impaired songs following unilateral but not bilateral lesions of nucleus uvaeformis of adult zebra finches. *J. Neurobiol.* **63**, 70–89 (2005).
13. Coleman, M. J., Roy, A., Wild, J. M. & Mooney, R. Thalamic gating of auditory responses in telencephalic song control nuclei. *J. Neurosci.* **27**, 10024–10036 (2007).
14. Danish, H. H., Aronov, D. & Fee, M. S. Rhythmic syllable-related activity in a songbird motor thalamic nucleus necessary for learned vocalizations. *PLoS ONE* **12**, e0169568 (2017).
15. Williams, H. & Vicario, D. S. Temporal patterning of song production: participation of nucleus uvaeformis of the thalamus. *J. Neurobiol.* **24**, 903–912 (1993).
16. Elmaleh, M., Kranz, D., Asensio, A. C., Moll, F. W. & Long, M. A. Sleep replay reveals premotor circuit structure for a skilled behavior. *Neuron* **109**, 3851–3861 (2021).
17. Nottebohm, F., Kelley, D. B. & Paton, J. A. Connections of vocal control nuclei in the canary telencephalon. *J. Comp. Neurol.* **207**, 344–357 (1982).
18. Akutagawa, E. & Konishi, M. New brain pathways found in the vocal control system of a songbird. *J. Comp. Neurol.* **518**, 3086–3100 (2010).
19. Mooney, R. & Prather, J. F. The HVC microcircuit: the synaptic basis for interactions between song motor and vocal plasticity pathways. *J. Neurosci.* **25**, 1952–1964 (2005).
20. Egger, R. et al. Local axonal conduction shapes the spatiotemporal properties of neural sequences. *Cell* **183**, 537–548 (2020).
21. Kornfeld, J. et al. EM connectomics reveals axonal target variation in a sequence-generating network. *eLife* **6**, e24364 (2017).
22. Long, M. A. & Fee, M. S. Using temperature to analyse temporal dynamics in the songbird motor pathway. *Nature* **456**, 189–194 (2008).
23. Picardo, M. A. et al. Population-level representation of a temporal sequence underlying song production in the zebra finch. *Neuron* **90**, 866–876 (2016).
24. Hahnloser, R. H., Kozhevnikov, A. A. & Fee, M. S. An ultra-sparse code underlies the generation of neural sequences in a songbird. *Nature* **419**, 65–70 (2002).
25. Kozhevnikov, A. A. & Fee, M. S. Singing-related activity of identified HVC neurons in the zebra finch. *J Neurophysiol.* **97**, 4271–4283 (2007).
26. Hamaguchi, K., Tanaka, M. & Mooney, R. A distributed recurrent network contributes to temporally precise vocalizations. *Neuron* **91**, 680–693 (2016).
27. Andalman, A. S., Foerster, J. N. & Fee, M. S. Control of vocal and respiratory patterns in birdsong: dissection of forebrain and brainstem mechanisms using temperature. *PLoS ONE* **6**, e25461 (2011).
28. Schmidt, M. F. Pattern of interhemispheric synchronization in HVc during singing correlates with key transitions in the song pattern. *J. Neurophysiol.* **90**, 3931–3949 (2003).
29. Valverde, S. et al. Deep brain stimulation-guided optogenetic rescue of parkinsonian symptoms. *Nat. Commun.* **11**, 2388 (2020).
30. Lymer, J., Prescott, I. A. & Levy, R. Microstimulation-induced inhibition of thalamic reticular nucleus in non-human primates. *Exp. Brain Res.* **237**, 1511–1520 (2019).
31. Arfin, S. K., Long, M. A., Fee, M. S. & Sarpeshkar, R. Wireless neural stimulation in freely behaving small animals. *J. Neurophysiol.* **102**, 598–605 (2009).
32. Vu, E. T., Mazurek, M. E. & Kuo, Y. C. Identification of a forebrain motor programming network for the learned song of zebra finches. *J. Neurosci.* **14**, 6924–6934 (1994).
33. Ashmore, R. C., Wild, J. M. & Schmidt, M. F. Brainstem and forebrain contributions to the generation of learned motor behaviors for song. *J. Neurosci.* **25**, 8543–8554 (2005).
34. Roberts, T. F. et al. Identification of a motor-to-auditory pathway important for vocal learning. *Nat. Neurosci.* **20**, 978–986 (2017).
35. Fee, M. S., Kozhevnikov, A. A. & Hahnloser, R. H. Neural mechanisms of vocal sequence generation in the songbird. *Ann. NY Acad. Sci.* **1016**, 153–170 (2004).
36. Scharff, C., Kirn, J. R., Grossman, M., Macklis, J. D. & Nottebohm, F. Targeted neuronal death affects neuronal replacement and vocal behavior in adult songbirds. *Neuron* **25**, 481–492 (2000).
37. Zhao, W., Garcia-Oscos, F., Dinh, D. & Roberts, T. F. Inception of memories that guide vocal learning in the songbird. *Science* **366**, 83–89 (2019).
38. Cardin, J. A., Raksin, J. N. & Schmidt, M. F. Sensorimotor nucleus Nlf is necessary for auditory processing but not vocal motor output in the avian song system. *J. Neurophysiol.* **93**, 2157–2166 (2005).
39. Otchy, T. M. et al. Acute off-target effects of neural circuit manipulations. *Nature* **528**, 358–363 (2015).
40. Vyssotski, A. L., Stepien, A. E., Keller, G. B. & Hahnloser, R. H. A neural code that is isometric to vocal output and correlates with its sensory consequences. *PLoS Biol.* **14**, e2000317 (2016).
41. Kosche, G., Vallentin, D. & Long, M. A. Interplay of inhibition and excitation shapes a premotor neural sequence. *J. Neurosci.* **35**, 1217–1227 (2015).
42. Cannon, J., Kopell, N., Gardner, T. & Markowitz, J. Neural sequence generation using spatiotemporal patterns of inhibition. *PLoS Comput. Biol.* **11**, e1004581 (2015).
43. Miri, A. et al. Spatial gradients and multidimensional dynamics in a neural integrator circuit. *Nat. Neurosci.* **14**, 1150–1159 (2011).
44. Reinke, H. & Wild, J. M. Identification and connections of inspiratory premotor neurons in songbirds and budgerigar. *J. Comp. Neurol.* **391**, 147–163 (1998).
45. Schmidt, M. F. & Wild, J. M. The respiratory–vocal system of songbirds: anatomy, physiology, and neural control. *Prog. Brain Res.* **212**, 297–335 (2014).
46. Johnson, M. D. & Ojemann, G. A. The role of the human thalamus in language and memory: evidence from electrophysiological studies. *Brain Cogn.* **42**, 218–230 (2000).
47. Jurgens, U. Neural pathways underlying vocal control. *Neurosci. Biobehav. Rev.* **26**, 235–258 (2002).
48. Pattinson, K. T. et al. Determination of the human brainstem respiratory control network and its cortical connections in vivo using functional and structural imaging. *Neuroimage* **44**, 295–305 (2009).
49. Wild, J. M. Visual and somatosensory inputs to the avian song system via nucleus uvaeformis (Uva) and a comparison with the projections of a similar thalamic nucleus in a nonsongbird, *Columba livia. J. Comp. Neurol.* **349**, 512–535 (1994).

Methods

Animals

We used adult (>90 days posthatch) male zebra finches (*Taeniopygia guttata*) that were obtained from an outside breeder and maintained in a temperature- and humidity-controlled environment with a 12-h light/12-h dark schedule. All animal maintenance and experimental procedures were performed according to the guidelines established by the Institutional Animal Care and Use Committee at the New York University Langone Medical Center.

Surgical procedures

All surgical procedures were performed under isoflurane anaesthesia (1–3% in oxygen) following established guidelines. To access Uva, the beak bar was positioned 5 degrees up from the horizontal and the electrode was inserted vertically. At this head angle, Uva coordinates varied from 1.5–1.7 mm lateral and 3.0–3.7 mm anterior from the bifurcation of the superior sagittal sinus and 5.1–5.5 mm ventral from the brain's surface. For all Uva-related manipulations (that is, lesions, chronic stimulation-electrode implantations and viral injections into Uva), Uva was confirmed antidromically through HVC stimulation. A platinum-iridium or tungsten search electrode (0.5 MΩ, MicroProbes) was used to measure spiking responses in Uva evoked by HVC stimulation (0.5 Hz, biphasic single pulse, 0.2 ms per phase, 100 µA). Stimulation was enabled using a bipolar electrode in HVC constructed from Teflon-coated stainless steel wire (0.002-inch California Fine Wire) inserted 2.3 mm lateral and 0.25 mm anterior from the bifurcation of the superior sagittal sinus with the beak bar at 45 degrees down from the horizontal.

Chronically implanted bipolar electrodes for lesions and microstimulation

We performed unilateral lesions acutely or chronically either in or adjacent to Uva, with the latter case categorized as a 'sham' condition. In some cases, lesions were made using custom-built bipolar stainless steel electrodes (0.002-inch California Fine Wire) inserted acutely into Uva during anaesthesia. In other cases, lesions were produced using custom bipolar electrodes composed of a platinum-iridium electrode (0.5 MΩ, MicroProbes, PI20030.5B3) and an insulated stainless steel wire (0.002-inch California Fine Wire) directly affixed to the platinum-iridium electrode using cyanoacrylate. The tips of the stainless steel and platinum-iridium wires were displaced vertically by approximately 400 µm. The platinum-iridium tip of this electrode allowed for unit recordings during implantation and therefore extremely precise, electrophysiology-guided placement in Uva. Unilateral lesions were achieved with 30-s biphasic pulses (acute: 50 µA, 6 total pulses; chronic: 50–500 µA, 6–10 total pulses). Lesion locations were confirmed histologically (details below). For all microstimulation experiments (Figs. 1 and 3), we used the latter platinum/iridium-type bipolar electrode with 0.001-inch stainless steel wire (California Fine Wire) displaced 220–300 µm vertically (Extended Data Fig. 3b). For behavioural microstimulation experiments (Fig. 1), both hemispheres were implanted with bipolar electrodes.

In vivo stereotaxic injections

Retrograde tracers. We used glass pipettes (opening diameter, 20 µm) with an oil-based pressure injection system (Nanoject III, Drummond Scientific) for all tracer and virus injections. For post hoc assessment of lesion success or stimulation electrode position, the ipsilateral HVC was injected with 200 nl of either dextran Alexa Fluor 488 (Invitrogen, D22910) or a virus (scAAV-DJ9-hCMV-chl-EGFP) to retrogradely label neurons projecting from Uva to HVC (Extended Data Fig. 4d–f). Counting HVC-projecting Uva neurons required dense labelling of the HVC-projecting Uva neuronal population. Therefore, we chose a two-tracer approach using EGFP[50] (Extended Data Fig. 4c) together with cholera toxin subunit B (100 nl; CTB, Alexa Fluor 647 conjugate; Invitrogen, C34778) (Extended Data Fig. 4b) and injected into the right hemisphere.

Axonal labelling. To label direct projections from Uva to HVC, we injected virus (AAV9-CAG-GFP; Addgene, 37825-AAV9) into two locations within Uva (62 nl per site), one at the ventral edge of Uva and one in its centre. To mark potential HVC postsynaptic targets, we sparsely labelled HVC–RA projection neurons with tdTomato. To accomplish this, we first electrophysiologically identified RA with a tungsten electrode (0.5 MΩ, MicroProbes) and injected 50 nl of a retrograde Cre-encoding virus diluted in physiological saline solution into its centre (1:20 dilution; scAAV-DJ9-hCMV-CRE)[50]. Then, 200 nl of Cre-dependent tdTomato virus (AAV9-FLEX-tdTomato; Addgene, 28306-AAV9) was injected into HVC.

GCaMP6s viral injections. We used viral vectors to express the calcium indicator GCaMP6s (AAV9-CAG-GCaMP6s-WPRE-SV40; Addgene, 100844) in either Uva or HVC. Uva injections were performed at two sites (ventral edge and centre, 62 nl of virus per site). To cover the entirety of HVC, we performed injections at 9 to 12 sites separated by approximately 250 µm in a grid-like fashion. At each point, we used either single injections at 400 µm below the brain's surface or two injections at 400 and 550 µm in depth. To minimize the impact on the tissue, HVC virus injections were performed with bevelled pipettes (opening diameter, 20 µm; length of bevel, 80–100 µm).

RetroBead injections. We injected red RetroBeads (Lumafluor) into Area X (two injection sites, 70 nl each). Area X was accessed through a small craniotomy centred at 1.5 mm lateral and 5.9 mm anterior to the superior sagittal sinus with the beak bar at 8 degrees up from the horizontal. Injections were made 2.8 mm below the brain's surface at 5.8 and 6.0 mm anterior (first and second injection, respectively) and 1.5 mm lateral. This procedure robustly labelled a large majority of basal ganglia-projecting HVC neurons (HVC_X) and allowed for unambiguous identification of this cell class during in vivo two-photon imaging.

Implantation of cranial windows

Cranial windows were placed above HVC for both axonal imaging of HVC-projecting Uva neurons and somatic imaging of HVC neurons. In each case, we carefully removed a circular piece of dura (diameter of approximately 1 mm) above HVC while leaving the transparent pia intact. The window was implanted at the end of the injection procedure (HVC injection) or 2 weeks after virus was injected (Uva injection). We sealed a 3-mm-diameter circular coverglass (#1 thickness, Warner Instruments) with Kwik-Sil adhesive (WPI) and fixed the edge of the glass with cyanoacrylate. We also cemented a black plastic ring (inner diameter, 5 mm; outer diameter, 7.5 mm) around the cranial window to prevent light contamination during imaging.

Head-fixed singing protocol

We habituated zebra finches to sing to a female while head-fixed, following a previously published protocol from our laboratory[23]. The female was initially visually occluded using a curtain that was lifted by a stepper motor (Wantai, model 57BYGH420-2) controlled by an Arduino (Arduino UNO with Arduino Motor Shield). We recorded female-directed singing with a lavalier condenser microphone (Audio-Technica, AT831) placed approximately 4 cm away from the beak of the head-fixed bird. The signal was amplified using a solid-state preamplifier (Behringer, Ultragain Pro MIC2200). Song was detected using a digital signal processor (RX8, Tucker-Davis Technologies), and custom software was written using the RPvdsEx interface (Tucker-Davis Technologies) and MATLAB to open a solenoid (NResearch) for 200 ms to dispense approximately 20 µl of water.

Article

Because the zebra finch produces a song containing short gaps between syllables and motifs, singing behaviour was defined as time periods in which the ratio of high-frequency power to low-frequency power (1–7 kHz and 0–1 kHz, respectively) was greater than 3 for more than 50% of a 1-s sliding window.

Two-photon imaging

We used a customized movable-objective microscope (Sutter Instrument) to scan our field of view (frame rate, 28.8 Hz) with a resonant system (Thorlabs) and ScanImage 4.2 software[51]. All imaging was done using a ×25 water-immersion objective (Olympus, XLPLN25XWMP) with a numerical aperture of 1.05 and a working distance of 2 mm. To protect the microscope from external light contamination, we wrapped it with a light-attenuating material. Additionally, we fit a black balloon to the tip of the objective on one end and the black ring surrounding the optical window on the other[52]. The excitation source was a mode-locked Ti:sapphire laser (Chameleon, Coherent) tuned at 920 nm and controlled by a Pockels cell (Conoptics, model 350-80; Controller 302RM). Fluorescent light was detected using a GaAsP photomultiplier tube (H10770PA-40 PMT module, Hamamatsu) and a wide detection path (2-inch collection lens).

To apply electrical stimulation to Uva while the ipsilateral HVC of a head-fixed bird was imaged, we connected the chronic stimulation electrode to a pulse generator (A-M Systems, model 2100). For a given imaging plane, Uva was stimulated >20 times at pseudo-random intervals (interval range, 2–4 s). Each stimulation event consisted of a train of five 100-µA bipolar, biphasic current pulses (0.2 ms per phase) delivered at 500 Hz. The stimulation-triggered activity of most cells was imaged in the awake non-singing bird or under ketamine anaesthesia (50 mg kg^{-1}, mixed with xylazine, 5 mg kg^{-1}).

Song-triggered microstimulation

Data related to gauging the behavioural impact of perturbing Uva activity with electrical stimulation were collected as part of the present study; HVC stimulation data were re-analysed from a previously published dataset[31]. For the Uva stimulation experiments, we tested the effectiveness of the chronically implanted stimulation electrodes under anaesthesia. A single electrical stimulus (biphasic current pulse, 0.2 ms per phase) was applied to Uva, separately for each hemisphere. Uva stimulation (5–50 µA) elicited orthodromic responses in the ipsilateral HVC, which we measured with a 0.5-MΩ tungsten electrode (MicroProbes) through an open craniotomy above HVC.

Once the electrode performance was confirmed, each bird was transferred into a sound-isolation chamber where singing was recorded with an omnidirectional microphone (Audio-Technica, AT803) and amplified with a tube preamplifier (Presonus, Studio Channel). We continuously monitored the sound inside the chamber with custom-written MATLAB software, which recorded singing in a sound-triggered manner. Simultaneously, the microphone signal was sent to a digital signal processor (RX8, Tucker-Davis Technologies). Custom software was written using the RPvdsEx interface (Tucker-Davis Technologies) to detect song and subsequently send out a TTL pulse to trigger stimulation consisting of a train of five bipolar, biphasic current pulses (0.2 ms per phase) delivered at 500 Hz (A-M Systems, model 2100); copying the previously established HVC stimulation protocol[31]. Stimulators were connected to the chronic Uva implants through a commutator (Doric Lenses, AERJ_12_HARW or Dragonfly, SL-88-10). The lowest stimulation current level necessary to truncate song in >80% of cases was established empirically for each bird. Stimulation currents were kept the same for each hemisphere. After an effective current level was established, we used this current level to stimulate during a minimum of 100 motifs per bird. To avoid more than one stimulation event per motif and to distribute stimulation times uniformly across the motif, a random delay was chosen, uniformly distributed between 0 and 1,200 ms, after which the trigger signal was sent. Following each stimulation, subsequent stimulations were blocked for 1.5 s.

Simultaneous microstimulation and silicon probe recordings

A high-density silicon probe (Diagnostic Biochips, 128-5) was lowered into HVC (2.25 mm lateral and 0.25 mm anterior to lambda), and a stainless steel ground wire (0.001-inch AM Systems) was inserted between the skull and the dura. Silicon elastomer (Kwik-Cast, WPI) was applied to the craniotomy once the target region was successfully identified (depth, ~0.4–0.7 mm). We stimulated locally (~100–200 µm) using a platinum-iridium electrode (0.5 MΩ, MicroProbes) in head-fixed, awake birds that were held in a foam restraint for the duration of the experiment. A biphasic current (five pulses of 100 µA at 500 Hz) was applied every 2–5 s for >100 trials. Neural data and TTL pulses time locked to the triggered stimulation were acquired using the Intan Recording Controller.

Histology

Brains were fixed through cardiac perfusion with PBS followed by 4% formaldehyde (PFA) in PBS. After removal, the brains were stored in PFA overnight and sliced at 50 µm (100 µm for electrode site verification) using a vibrating microtome (VT1200S, Leica). Slices were mounted on microscope slides (Fisher Scientific, Colorfrost Plus) with Vectashield Antifade mounting medium with DAPI staining (Vector Laboratories). We imaged using a Zeiss confocal microscope (Axio ObserverZ1, LSM800) and took tiled image stacks (z step of 1 µm or 0.5 µm) for Uva cell counting and axonal images. For electrode site verification, we used an Olympus fluorescence microscope (BX53).

To detect Uva axons and potential postsynaptic targets in HVC, birds were perfused 2–3 weeks after injection. Slices were incubated in a blocking solution containing 0.2 g BSA, 10% normal donkey serum and 0.5% Triton X-100 for 1 h at room temperature. Slices were then incubated in blocking solution containing anti-GFP (1:1,000; ThermoFisher, A-11122) and mouse anti-NeuN (1:500; Sigma, MAB377). After rinsing three times for 10 min each using PBS, slices were transferred to secondary antibodies, specifically anti-mouse AF647 and anti-rabbit AF488 (1:1,000; ThermoFisher, A-32787 and A-21206, respectively), for 2 h at room temperature. Slices were then rinsed three times for 10 min each and mounted using Vectashield Antifade mounting medium (Vector Laboratories). In another case, slices were stained for GFP, as described above, and for tdTomato using goat anti-tdTomato (1:200; OriGene, AB8181-200) and anti-goat AF594 (1:1,000; ThermoFisher, A-11058) as the secondary antibody.

To quantify the number of HVC-projecting Uva neurons, birds were perfused 6 days after injection. Slices were blocked with the same protocol as described above and then rinsed with PBS three times for 10 min each before incubation with anti-mouse AF555 secondary antibody (1:1,000; ThermoFisher, A-31570) for 2 h at room temperature. Slices were then rinsed three times for 10 min each in PBS and mounted using Vectashield. Manual cell counting analysis was performed using Amira Software.

Data analysis: behavioural effects of Uva lesions

We recorded the songs of birds 1–12 days following Uva lesions. To determine lesion-induced changes to the structure of vocal elements, we used principal-component analysis (PCA). First, vocalizations were manually annotated by identity (that is, syllable A, syllable B). For each bird, all segments were zero padded to match the length of the longest syllable. Spectrograms were then embedded using PCA in MATLAB, restricting our analysis to the first five PCs. Clusters were determined using k-means clustering for k = 2–10 and scored using silhouette analysis, which requires a minimum of two clusters. Distances were calculated using cosine distance to ensure the measure was invariant to rescaling of the data. Barnes–Hut t-SNE was used to visualize the distributions of vocal elements before and after lesion. Spectrograms

(processed as described above) for both pre- and postlesion vocalizations were analysed using an established *t*-SNE algorithm (perplexity hyperparameter = 45)[53].

Data analysis: microstimulation perturbation of singing behaviour

For all song recordings, if stimulation onset times fell within the range of one of the bird's song motifs (that is, from 50 ms before motif onset to the end of the motif), we manually annotated the start and stop time of all syllables, including truncated syllables. The ends of syllables were defined as the times at which the amplitude fell back to baseline. We used a custom graphical user interface for syllable annotations, which allowed for detailed spectrogram and raw audio inspection. The motif stop time was defined by the final syllable produced. For each bird, a representative reference motif was chosen, and the syllables of every individual motif were aligned to the corresponding syllable onsets of the reference motif. To avoid motif stop times unrelated to stimulation, we excluded stop times that happened after the length of the reference motif minus 30 ms from further analysis. We used a Kruskal–Wallis test to ask whether aligned Uva and HVC motif stop times came from the same distribution. To visualize and normalize truncation probabilities across individual birds, aligned stop times were smoothed with a sliding average (window, 10 ms; step size, 1 ms) and divided by the total number of truncations.

Data analysis: simultaneous microstimulation and silicon probe recordings

Custom MATLAB software was used to analyse recordings and to align single-unit data to stimulation times. Automated spike detection and sorting was carried out using Kilosort software[54] and manual postprocessing was performed using Phy[55] as described previously[20]. Peristimulus time histograms were calculated using either 5-ms bins (Extended Data Fig. 2a–c) or 25-ms bins (Extended Data Fig. 2c). Spike histograms were normalized by the maximum firing rate during the 2-s window centred on the stimulus. Neurons were classified as stimulus activated if they met our criterion: $fr_{stim}/fr_{pre} - fr_{stim} < 0$ (where fr is the firing rate; prestimulus window = −1,000 to 0 ms; stimulus window = 0 to 200 ms). Waveforms were measured for all spike times occurring in the 1 s before stimulus onset with rise time calculated as the time to reach 90% of the maximum peak–trough amplitude.

Data analysis: two-photon imaging

For both soma and axon imaging experiments, we used multichannel analog-to-digital converter (Digidata 1550, Molecular Devices) and Clampex software (pCLAMP, v.9) to synchronize the microphone and stimulation trigger signal with the start and stop time of each frame acquisition (frame resolution, 512 × 512 pixels; frame size, 228 × 228 μm^2 or 341 × 341 μm^2 for somatic imaging and 137 × 137 μm^2 for axonal imaging). We defined the scan time for each individual frame-line as the moment that a line's central pixel was recorded. We motion corrected all acquired images within and across trials using a non-rigid motion correction algorithm (NoRMCorre)[56,57]. Following motion correction, ROIs were manually drawn, and the fluorescence of each ROI was estimated using freely available software (ImageJ). Fluorescence traces were extracted by taking the mean pixel value within the respective ROIs, and each ROI's scan time was defined as the scan time of its central line. Because of the stability of zebra finch song-motor coding across time[58], we matched ROIs across days in cases where the same ROI was recorded in more than one session. Next, we segmented and labelled all song motifs, introductory notes, distance calls and tet calls using custom MATLAB software. Given the slight variability in song timing across trials[9,20], it was necessary to linearly warp the vocalizations to a uniform duration. For each vocalization, we applied an identical warp factor to the corresponding scan times. Finally, for each ROI and trial, we defined as baseline (*F*) the average of 250 samples before the curtain was lifted and calculated $\Delta F/F$.

Neurons labelled with red RetroBeads injected into Area X were defined as basal ganglia-projecting (that is, HVC_X) neurons. HVC premotor neurons (that is, HVC_{RA} neurons) were defined as cells without RetroBead labelling and with at least one stereotyped, vocalization-locked phasic fluorescence increase. The remainder of imaged neurons, distinguished by the absence of a retrograde tracer and the lack of a stereotyped, vocalization-locked phasic fluorescence increase, may represent either HVC interneurons or Av-projecting neurons.

The onset times of phasic fluorescence increases in HVC premotor neurons were previously shown to correspond to the burst onset times (that is, spiking events) of these neurons[23]. We deconvolved the onset times of HVC_{RA} neurons using a Markov chain Monte Carlo (MCMC) inference method[23]. In brief, the MCMC chain was run for 5,000 sweeps over all parameters (with a burn-in of 2,000 sweeps). The burst onset time was defined as the median onset estimate and uncertainty as the standard deviation of the last 3,000 sweeps.

Data analysis: Uva stimulation-evoked $\Delta F/F$

To quantify the fluorescence increase of individual HVC neurons following electrical microstimulation in Uva, we compared single-cell fluorescence before and after stimulation. In a first step, we subtracted local background fluorescence. Specifically, for a given somatic ROI, we generated an annulus ROI surrounding the somatic ROI while excluding close by other somatic ROIs. The area of the annulus was 20 times the area of the corresponding somatic ROI. The mean pixel value of the annulus was subtracted from the mean pixel value of the somatic ROI for each sample. After background correction, we quantified fluorescence changes on a trial-by-trial basis. For each stimulation event, we tested whether 15 samples of fluorescence values (approximately 500 ms) following the stimulation were significantly larger than the 15 samples before the stimulation (one-tailed Wilcoxon test, $P < 0.01$). The sum of stimulations followed by a significant fluorescence increase was then divided by the total number of stimulations to obtain an 'activation ratio' for each individual neuron. Additionally, we calculated $\Delta F/F$, individually for each stimulation, using the mean fluorescence across the 500 ms preceding a stimulation as baseline (*F*). The average $\Delta F/F$ across the 500 ms following stimulation, across all stimulations, was then calculated to obtain a single post-stimulation $\Delta F/F$ value for each neuron. Most HVC neurons were observed during two Uva stimulation conditions, under ketamine anaesthesia and in the awake bird. For these cells, the condition with the maximum activation ratio and $\Delta F/F$ was selected for further analysis. We then used a *k*-means clustering algorithm on the activation ratios and $\Delta F/F$ values of all premotor neurons to assign each cell to one of two clusters. Specifically, we used the sum of absolute differences, where each centroid was the component-wise median of the points in its cluster (MATLAB, k-means function; distance measure, 'cityblock'). We refer to these two clusters as Uva-driven (UvD) and not Uva-driven (nUvD) HVC premotor neurons.

Data analysis: comparison of HVC premotor neuron spiking event times

We used the amplitude envelope of each bird's reference motif (that is, the song motif we used for linear time warping; see above) to calculate an event-triggered median song amplitude. For each reference motif, we calculated a sliding root-mean-square (r.m.s.; window, 3.7 ms; step size, 25 μs) level and then divided by the 99th percentile of the motif's r.m.s. values to normalize amplitudes. These amplitude envelopes were then used to cut and align a 100-ms envelope cutout to each HVC premotor neuron spiking event (−25 to +75 ms relative to event time). For each cutout, the minimum amplitude was subtracted, and envelope edges were zero padded to account for event times at the onset or offset of the motif. Median event-aligned amplitude envelopes were calculated for UvD and nUvD HVC premotor neuron populations. Next, we took a bootstrapping approach to calculate a distribution of median event-aligned amplitude envelopes separately for UvD and

Article

nUvD premotor neuron populations. For each bird, we generated a random uniform distribution of time points matching the number of actual UvD or nUvD spiking events of a given bird and derived a 100-ms amplitude envelope cutout for each of those time points. We then registered the median of these amplitude envelopes across all birds and repeated this procedure 100,000 times to arrive at a distribution of median event-aligned amplitude envelopes. Finally, we compared the 99% confidence interval of these distributions to our data (UvD and nUvD separately).

To align premotor neuron spiking events to the onset or offset of song syllables, introductory notes or calls, we manually labelled those time points for all vocalizations. Syllable boundaries were defined as points where song amplitude fell to baseline for a minimum of 10 ms to include all inspiratory gaps, which typically range between 20–50 ms[45]. We then aligned all premotor neuron spiking events that happened within ±50 ms relative to a vocal onset or offset to the closest onset and offset. These relative time points were assigned to 1-ms bins; their distribution was smoothed with a sliding average (window, 10 ms; step size, 1 ms) and divided by the total number of time points to obtain a normalized distribution of firing probabilities, separately for UvD and nUvD time points. Finally, taking a bootstrapping approach, we asked whether those distributions exceeded the 99% confidence interval of a uniform distribution. We generated a uniform distribution of time points by the random assignment of a number of time points matching the actual UvD or nUvD time points within our ±50-ms window into 100 bins (bin size, 1 ms). This random uniform distribution was then smoothed with a sliding average as described above. We repeated this step 100,000 times to obtain a distribution of uniform time point distributions and calculated the 99% confidence interval for each 1-ms bin.

Data analysis: Uva$_{HVC}$ axon activity

To quantify the responses of HVC-projecting Uva axons in HVC, we looked at the fluorescence modulation ($\Delta F/F$) of individual axonal ROIs relative to the onset of vocalizations (song, introductory notes, distance calls and tet calls). If two or more axonal ROIs on a given plane showed the same activity profile, they were joined to one ROI, resulting in 13 axonal ROIs. An ROI was defined as significantly modulated relative to a given vocalization type if at least 10 renditions of this vocalization were collected and if the mean $\Delta F/F$ across the 400-ms window preceding vocalization onset was significantly different from the mean $\Delta F/F$ across the 400-ms window following vocalization onset across all renditions (two-sided paired Wilcoxon test, $P < 0.01$). For single song motifs and song bouts (that is, several repeated song motifs in a row), the analysis deviated from this standard procedure as follows: the 400 ms before bout onset was used as a reference for every motif in the bout. This reference was then compared to a 400-ms window, sliding over a given motif in 100-ms steps. For example, if the motif had a length of 600 ms, six comparisons were made with the reference window and alpha was Bonferroni corrected accordingly. If at least one comparison was significant, the ROI was defined as significantly modulated by song.

To visualize modulation strength and direction (that is, fluorescence increase or decrease) for all significant modulations, we calculated a modulation index. Here we asked, for each individual rendition of one vocalization type, whether a ROI's mean $\Delta F/F$ across the 400 ms before vocalization onset was significantly different from the mean $\Delta F/F$ across a 400-ms window following vocalization onset. If there was no significant difference, we registered a 0. If there was a significant increase in fluorescence, we registered a 1. If there was a significant decrease, we registered a −1. The sum of the resulting vector was then divided by the total number of renditions to obtain a value between −1 and 1, that is, the modulation index.

Throughout the main text, average values are given with standard deviation unless otherwise noted. No statistical method was used to predetermine sample size. The datasets and analysis code generated from the current study are available from the corresponding author on request.

Reporting summary

Further information on research design is available in the Nature Portfolio Reporting Summary linked to this article.

Data availability

The data that support the findings of this study are available from the corresponding author upon request.

50. During, D. N. et al. Fast retrograde access to projection neuron circuits underlying vocal learning in songbirds. *Cell Rep.* **33**, 108364 (2020).
51. Pologruto, T. A., Sabatini, B. L. & Svoboda, K. ScanImage: flexible software for operating laser scanning microscopes. *Biomed. Eng. Online* **2**, 13 (2003).
52. Dombeck, D. A., Harvey, C. D., Tian, L., Looger, L. L. & Tank, D. W. Functional imaging of hippocampal place cells at cellular resolution during virtual navigation. *Nat. Neurosci.* **13**, 1433–1440 (2010).
53. Kollmorgen, S., Hahnloser, R. H. R. & Mante, V. Nearest neighbours reveal fast and slow components of motor learning. *Nature* **577**, 526–530 (2020).
54. Pachitariu, M., Steinmetz, N., Kadir, S., Carandini, M. & Kenneth, D. H. Kilosort: realtime spike-sorting for extracellular electrophysiology with hundreds of channels. Preprint at *bioRxiv* https://doi.org/10.1101/061481 (2016).
55. Rossant, C. et al. Spike sorting for large, dense electrode arrays. *Nat. Neurosci.* **19**, 634–641 (2016).
56. Guizar-Sicairos, M., Thurman, S. T. & Fienup, J. R. Efficient subpixel image registration algorithms. *Opt. Lett.* **33**, 156–158 (2008).
57. Pnevmatikakis, E. A. & Giovannucci, A. NoRMCorre: an online algorithm for piecewise rigid motion correction of calcium imaging data. *J. Neurosci. Methods* **291**, 83–94 (2017).
58. Katlowitz, K. A., Picardo, M. A. & Long, M. A. Stable sequential activity underlying the maintenance of a precisely executed skilled behavior. *Neuron* **98**, 1133–1140 (2018).

Author contributions F.W.M. and M.A.L. conceived the study and designed the experiments; F.W.M., M.E., L.A.A.-S., D.K. and A.C.A. conducted the research; F.W.M., M.E., L.A.A.-S. and M.A.L. performed data analyses; F.W.M., L.A.A.-S., A.C.A. and M.A.L. created the figures; F.W.M. and M.A.L. wrote the initial draft of the manuscript; F.W.M., M.E., A.C.A. and M.A.L. edited and reviewed the final manuscript. M.E. and M.A.L. acquired funding; M.A.L. supervised the project.
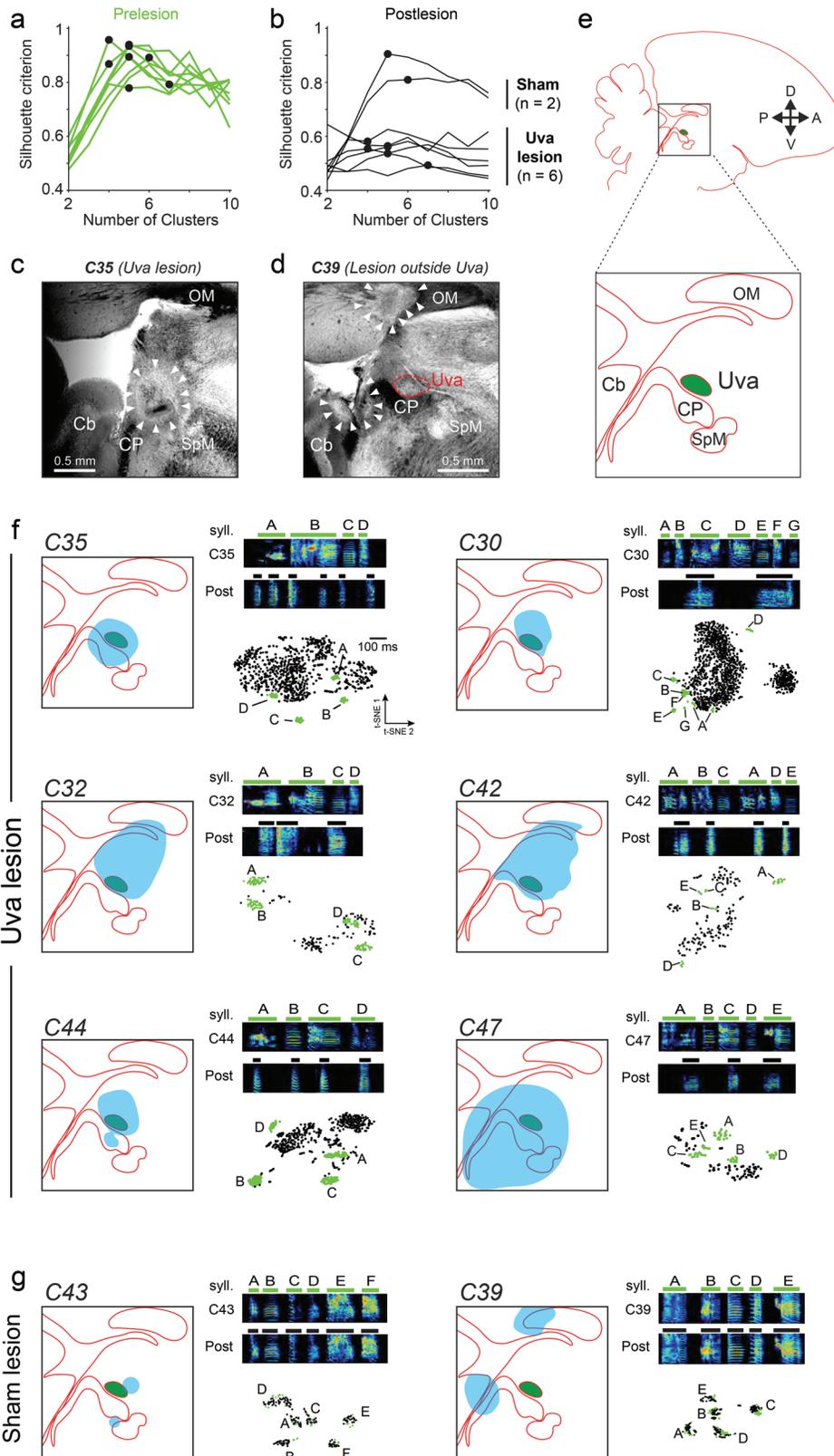
Extended Data Fig. 1 | Uva lesions impact syllabic song structure.
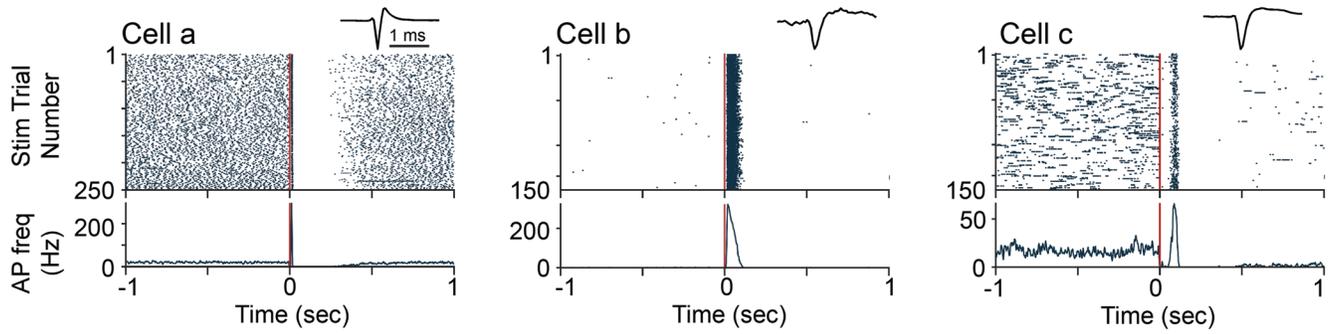**a**,**b**, Silhouette criteria calculated on the prelesion (**a**) and postlesion
(**b**) vocalizations for each bird (n = 8) for k-means of various sizes embedded
using the first five PCs. Black circles superimposed on curves indicate the
number of syllables in each bird's song motif. **c**,**d**, Histology of Uva lesioned
(n = 6) (**c**) and sham lesioned (n = 2) (**d**) birds (brightfield images, sagittal slices).
White arrows indicate the extent of the lesions. CP: Posterior commissure, OM:
occipitomesencephalic tract, SpM: nucleus spiriformis medialis,

Cb: cerebellum. **e**, Schematic of the zebra finch brain at the medio-lateral
level of Uva (sagittal view) based on an established anatomical resource
(http://www.zebrafinchatlas.org/). The highlighted region is used in (**f**) and
(**g**) to show the lesion extent (in transparent blue) for individual birds. **f**, **g**, *t*-SNE
plots representing vocalizations taken from Uva lesioned (**f**) and sham lesioned
(**g**) birds (prelesion green, postlesion black). Example sonograms depict
pre- and postlesion song motifs.

a, Transiently active neurons

Cell a, Cell b, Cell c

b Suppressed neurons

Cell i, Cell ii, Cell iii

c Transiently active neurons (n = 14)

Suppressed neurons (n = 50)

Rel. AP Rate

d Spike kinetics (90% rise time)
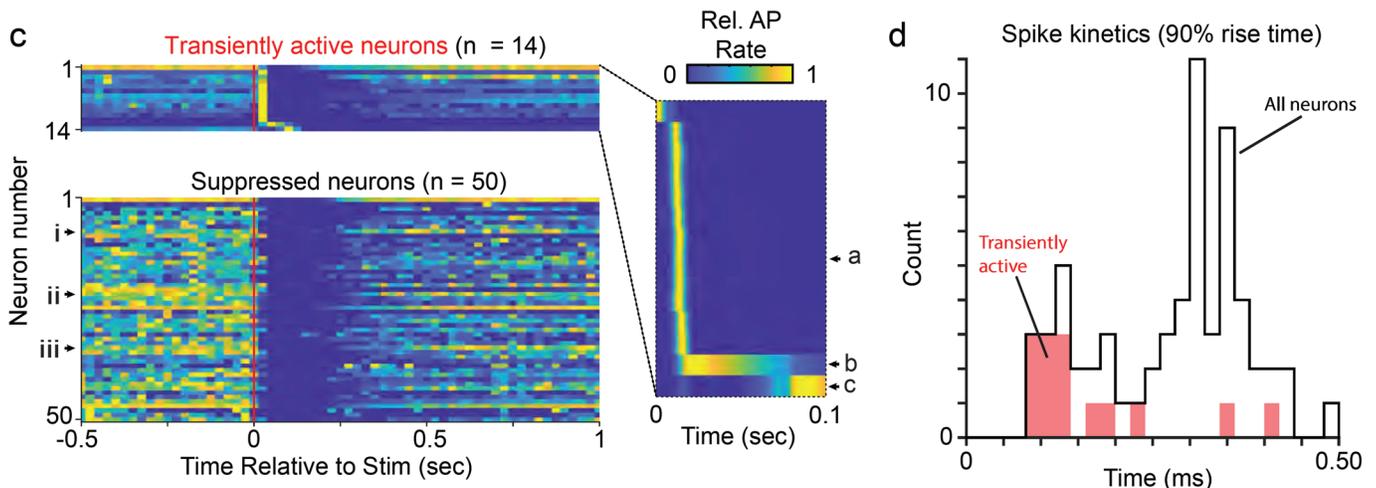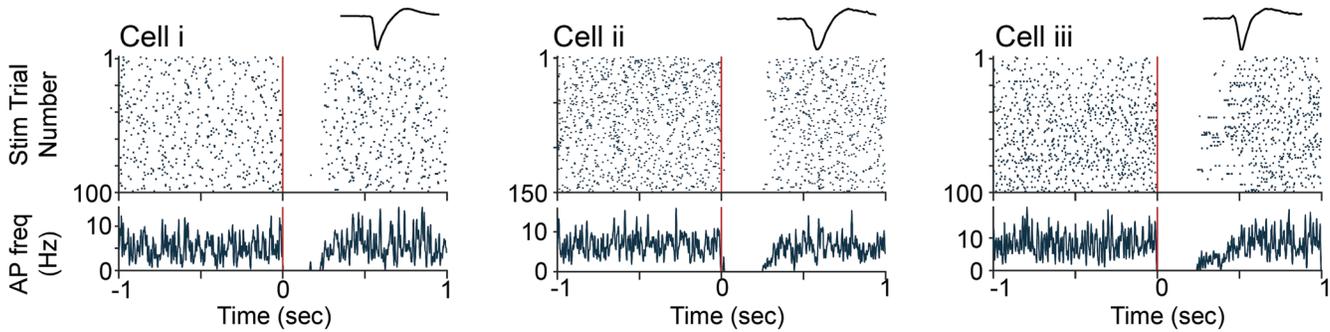
Extended Data Fig. 2 | Circuit-level consequences of electrical stimulation.
a,b, Example spike rasters (top) and peristimulus time histograms (bottom) for 6 HVC neurons that respond transiently **(a)** or are suppressed **(b)** by local high-frequency stimulation (see Methods). Red line indicates the onset of stimulation. Intensity and timing of stimulation identical to that used in behavioral experiments (i.e., Fig. 1). Inset: Average waveform for each neuron shows a variety of spike widths (Spike rise times - Cell a: 0.09 ms, Cell b: 0.34 ms,

Cell c: 0.20 ms, Cell i: 0.36 ms, Cell ii: 0.41 ms, Cell iii: 0.30 ms. **c**, Activity profiles of 64 neurons recorded during local stimulation from 2 birds (bin size: 25 ms). At right, a closer view of responses from transiently active neurons (bin size: 5 ms). Color scale ranges from 0 (no firing) to 1 (maximum firing rate during observation period). **d**, Histogram showing the spike rise times (see Methods) for all recorded neurons. Transiently active neurons (red) often displayed shorter rise times, indicative of inhibitory interneurons.
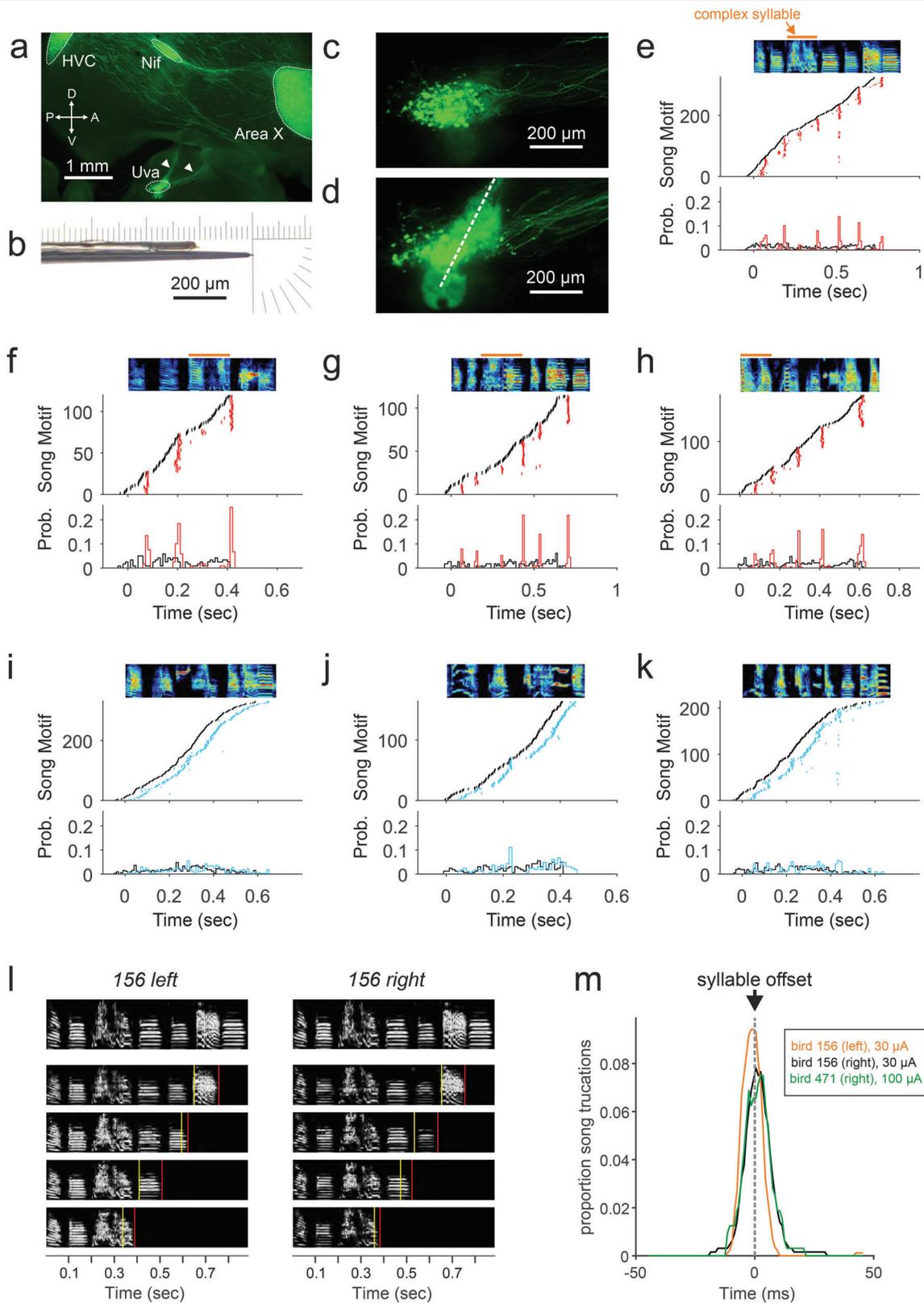
**Extended Data Fig. 3** | See next page for caption.

Article

Extended Data Fig. 4 | Quantifying the population of HVC-projecting Uva neurons. a–c, Sagittal view of HVC (white dotted line) into which retrograde tracers were injected (right is anterior) (n = 3 birds). NeuN labeled neurons shown in orange (**a**). Extent of fluorescently labeled cholera toxin subunit B (red) relative to HVC (**b**). Local labeling of cells with EGFP (green) after the injection of a retrograde virus into HVC (**c**). **d–f**, Spheres indicate retrogradely labeled HVC-projecting Uva neurons from three zebra finches shown in parasagittal (**d**), coronal (**e**), and transverse (**f**) views. Scale bars: 200 μm.
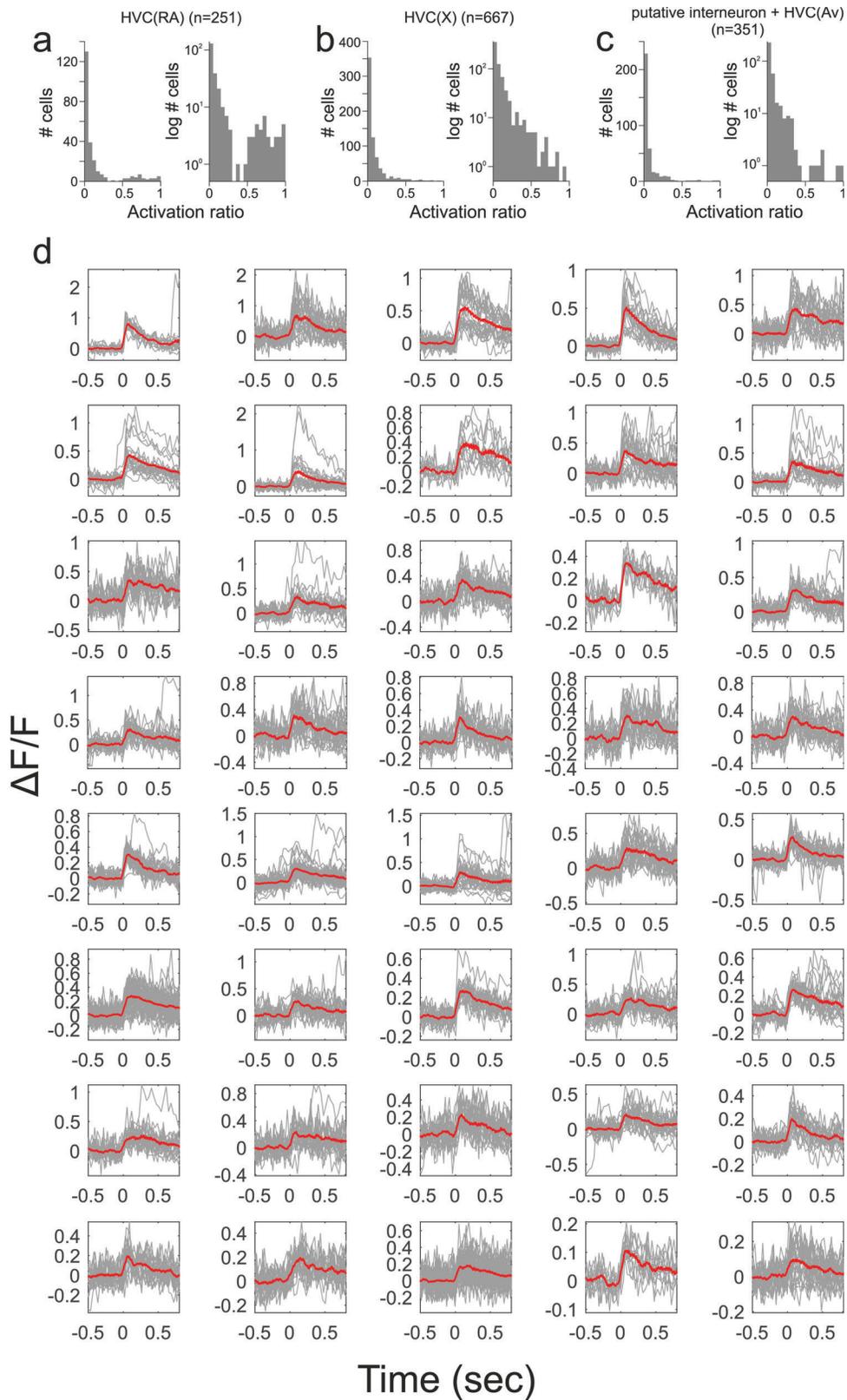
Extended Data Fig. 5 | Uva-stimulation responses in each HVC cell type.
a–**c**, Activation ratios following Uva stimulation for premotor neurons (HVC$_{RA}$)
(**a**), basal ganglia-projecting neurons (HVC$_X$) (**b**), and putative interneurons
(HVC$_{Int}$) and Avalanche-projecting neurons (HVC$_{Av}$) (**c**). Left histogram same
data as plots at right but on a logarithmic axis. **d**, Individual (gray) and average
(red) fluorescence changes following Uva stimulation for each Uva driven
HVC$_{RA}$ neuron from Fig. 3g.
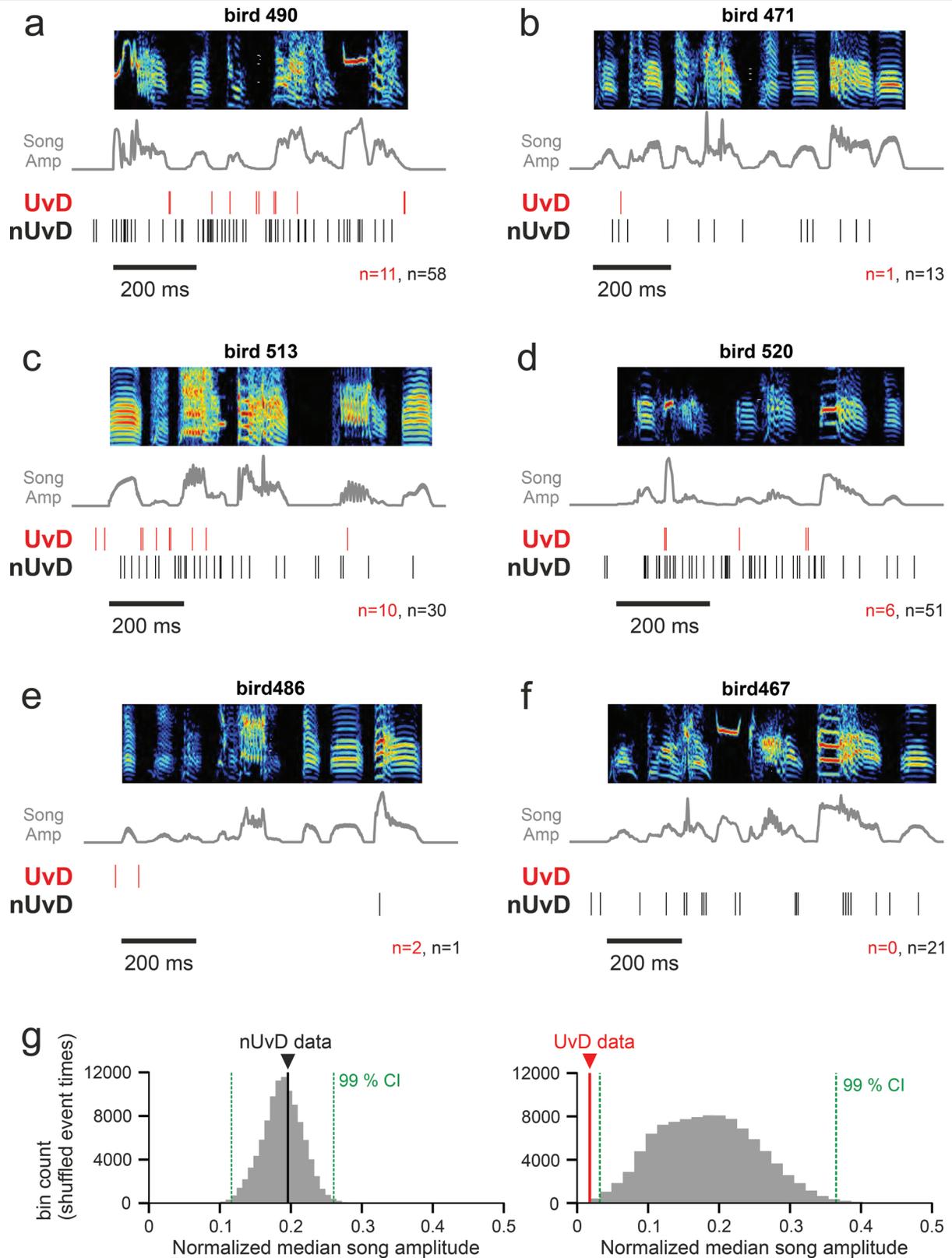
Extended Data Fig. 6 | UvD and nUvD spiking event times relative to song for premotor neurons across all birds. a–f, All spiking event times for UvD and nUvD neurons across all birds aligned to sonogram and amplitude of song motif. Bird 490 (UvD = 11, nUvD = 58) (**a**), Bird 471 (UvD = 1, nUvD = 13) (**b**), Bird 513 (UvD = 10, nUvD = 30) (**c**), Bird 520 (UvD = 6, nUvD = 51) (**d**), Bird 486 (UvD = 2, nUvD = 1) (**e**), Bird 467 (UvD = 0, nUvD = 21) (**f**). **g**, Comparison of song amplitude following UvD and nUvD spiking events. nUvD (black) and UvD (red) lines show the median song amplitude following spiking events for recorded data (window: 4 to 19 ms post spiking event; nUvD, n = 174, UvD, n = 30) compared with a 99% confidence interval (CI) based on the distribution of 100,000 median song amplitude values (same window) drawn from data matched numbers of uniformly distributed, random event times (see Methods).
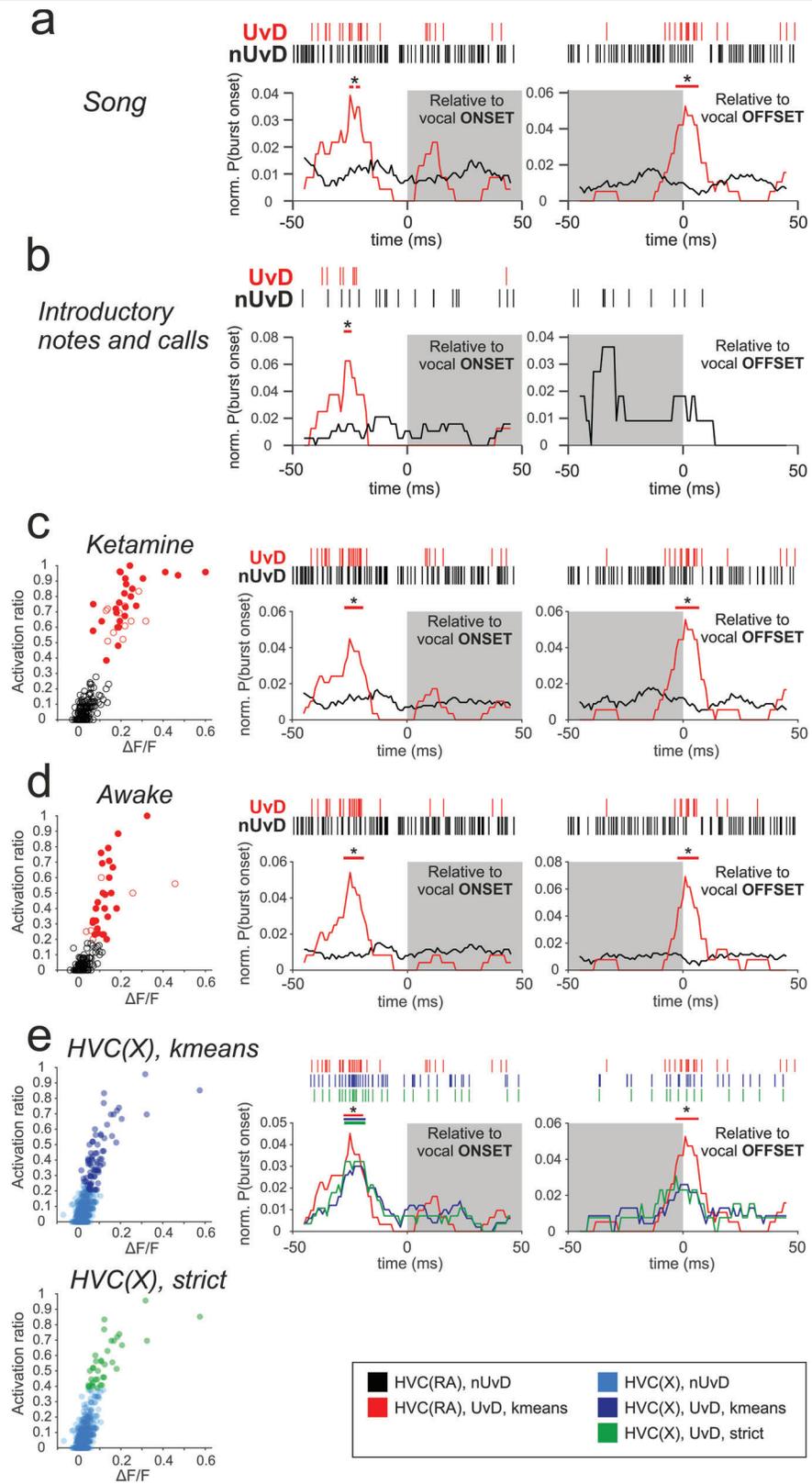
Extended Data Fig. 7 | See next page for caption.

Extended Data Fig. 7 | Spiking event times of UvD and nUvD HVC$_{RA}$ and HVC$_X$ neurons aligned to vocalization onset and offset. a, Spiking event times of HVC$_{RA}$ neurons active during singing. Left: Aligned to the closest syllable onset (UvD, n = 23; nUvD, n = 106). Right: Aligned to the closest syllable offset (UvD, n = 19; nUvD, n = 89). **b**, Spiking event times of HVC$_{RA}$ neurons active during introductory notes, distance calls, or tet calls. Left: Aligned to the closest vocalization onset (UvD, n = 8, nUvD, n = 19). Right: Aligned to the closest vocalization offset (UvD, n = 0, nUvD n = 11). No spiking events from UvD HVC$_{RA}$ neurons were found within 50 ms of introductory note or call offsets. **c**, Left: Scatterplot displaying activation ratios and Uva stimulation evoked ΔF/F for 227 HVC$_{RA}$ neurons observed in the ketamine condition. Filled circles in the UvD cluster (red) were also classified as UvD cells in the awake condition shown in (**d**). Middle: Spiking event times of HVC$_{RA}$ neurons – classified based on the ketamine condition – aligned to the closest syllable onset (UvD, n = 29; nUvD, n = 114). Right: Aligned to the closest syllable offset (UvD, n = 18; nUvD, n = 90).

d, Left: Same as (**c**) for 220 HVC$_{RA}$ neurons observed in the awake condition. Filled circles in the UvD cluster (red) were also classified as UvD cells in the ketamine condition shown in (**c**). Middle: Spiking event times of HVC$_{RA}$ neurons – classified based on the awake condition – aligned to the closest syllable onset (UvD, n = 24; nUvD, n = 113). Right: Aligned to the closest syllable offset (UvD, n = 13; nUvD, n = 88). **e**, Left: Scatterplot displaying activation ratios and Uva stimulation evoked ΔF/F for 667 HVC$_X$ neurons. Neurons were classified using either *k*-means clustering (top) or a 'strict' activation ratio threshold (bottom), which was set to 0.38 (i.e. the lowest activation ratio of the UvD cluster in Fig. 3g). Middle: Spiking event times of UvD HVC neurons aligned to the closest syllable onset (*k*-means: HVC$_{RA}$, n = 31; HVC$_X$, n = 50; strict: HVC$_X$, n = 28). Right: Aligned to the closest syllable offset (*k*-means: HVC$_{RA}$, n = 19; HVC$_X$, n = 23, strict: HVC$_X$, n = 13). Horizontal red, green or blue lines indicate moments in which the population exceeds a 99% CI of a uniform distribution.